Supermultiplexed optical imaging and barcoding with engineered polyynes

Fanghao Hu[1,3], Chen Zeng[1,3], Rong Long[1], Yupeng Miao[1], Lu Wei[1], Qizhi Xu[1] & Wei Min[1,2]

Optical multiplexing has a large impact in photonics, the life sciences and biomedicine. However, current technology is limited by a 'multiplexing ceiling' from existing optical materials. Here we engineered a class of polyyne-based materials for optical supermultiplexing. We achieved 20 distinct Raman frequencies, as 'Carbon rainbow', through rational engineering of conjugation length, bond-selective isotope doping and end-capping substitution of polyynes. With further probe functionalization, we demonstrated ten-color organelle imaging in individual living cells with high specificity, sensitivity and photostability. Moreover, we realized optical data storage and identification by combinatorial barcoding, yielding to our knowledge the largest number of distinct spectral barcodes to date. Therefore, these polyynes hold great promise in live-cell imaging and sorting as well as in high-throughput diagnostics and screening.

Multiplexing techniques allow simultaneous measurement of a large number of distinctive species. Applications include, for example, imaging multiple proteins or organelles with probes of different colors[1–3]; cell phenotyping, sorting and tracing[4]; high-throughput detection of antigens for medical diagnostics or small molecules for drug discovery[5–7]; and high-density information storage and encryption for identity security and anticounterfeiting[8,9]. As optical methods offer spectral features that can be identified in a noninvasive and nondestructive manner, optical multiplexing is making a broad impact in photonics, biology and medicine.

Materials are at the core of multiplexing technology, and many multiplexable optical materials have been developed. Organic dyes and fluorescent proteins are widely applied for multicolor imaging in biology[1], and inorganic materials including quantum dots, noble metal nanostructures, rare-earth nanoparticles and upconversion nanocrystals are used in spectral barcoding for high-throughput screening[7,9]. However, because of the intrinsically broad linewidth and/or significant spectral overlap, the number of resolvable features is limited. No more than six colors can be imaged in live cells, even by sophisticated fluorescence microscopy[2]. And fewer than 2,000 spectral barcodes can be practically reached[10] on account of unavoidable cross-talk in organic dyes, energy transfer between quantum dots[11,12] and limited number of suitable features for straightforward decoding in rare-earth nanocrystals and metal nanoparticles[9,13,14]. Yet, more colors and barcodes are essential for next-generation multiplexing. Therefore, new optical materials are needed to overcome the spectral limitation and break the 'multiplexing ceiling'.

We report the development of new polyyne-based materials and exploit their optical properties for supermultiplexed encoding and detection. Polyyne is a linear chain of sp-hybridized carbon atoms with alternating single and triple bonds, and it is also known as the carbon-atom wire[15]. Compared to other carbon materials such as sp^3-hybridized diamond and sp^2-hybridized graphene, carbon nanotube and fullerene, sp-hybridized polyyne is one of the least studied carbon allotropes with true 1D structure[16]. Although theory predicts them with appealing physical properties, such as high thermal conductivity and mechanical properties such as tensile stiffness and specific strength[15,17], difficulties in accessing stable polyynes have hindered their exploration. Recently, progress has been made toward the chemical synthesis of polyynes with well-defined composition, and a polyyne with 44 contiguous carbon atoms was successfully synthesized[18]. Here, we apply engineered polyynes to supermultiplexed optical imaging and barcoding.

RESULTS

Raman spectroscopy of phenyl-capped polyynes

We first synthesized a series of polyynes with phenyl end-capping groups (**Supplementary Note**). Using Glaser–Hay and Cadiot–Chodkiewicz coupling[19], we developed an efficient and robust route to prepare both odd- and even-numbered polyynes with two to six triple bonds (C≡C) (**Fig. 1**). A polar hydroxymethyl group is introduced on the phenyl ring for facile purification and serves as an active site for subsequent functionalization. UV-Vis spectra show the longest wavelengths of absorption in polyynes shift from UV (337 nm) to visible (476 nm) region with clear vibronic progression (**Supplementary Fig. 1**), as the length increases from 2-yne to 6-yne with lowered HOMO-LUMO bandgap. All polyyne

[1]Department of Chemistry, Columbia University, New York, New York, USA. [2]Kavli Institute for Brain Science, Columbia University, New York, New York, USA. [3]These authors contributed equally to this work. Correspondence should be addressed to W.M. (wm2256@columbia.edu).

RECEIVED 23 AUGUST 2017; ACCEPTED 5 DECEMBER 2017; PUBLISHED ONLINE 15 JANUARY 2018; DOI:10.1038/NMETH.4578

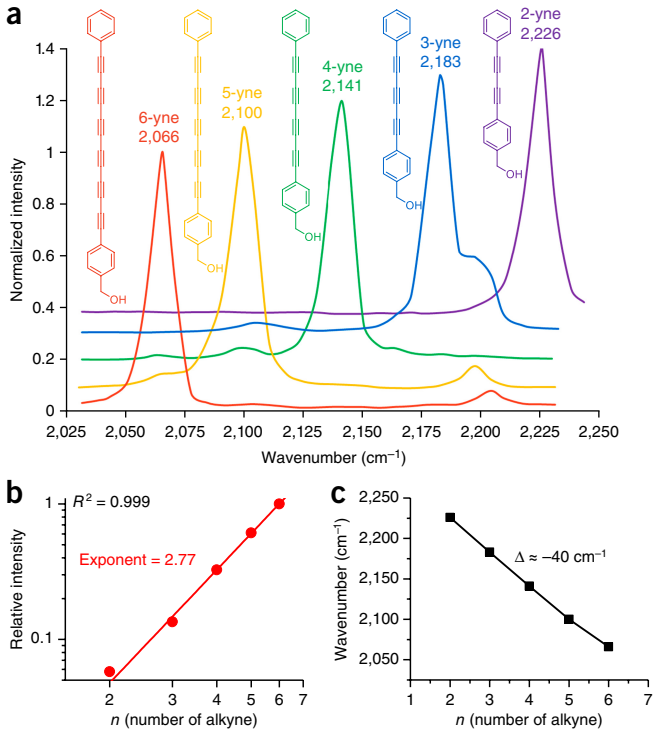

Figure 1 | Raman spectroscopy of phenyl-capped polyynes. (**a**) Normalized Raman spectra of polyynes from 2-yne to 6-yne and their structures. The spectra are vertically offset for clarity. (**b**) Raman peak intensity of polyynes as a function of the conjugation length. Solid line shows a power function fitting in the double logarithmic plot (R^2 = 0.999, n = 5 compounds). (**c**) Raman frequency of polyynes as a function of length, with an interval of ~40 cm^{-1}.

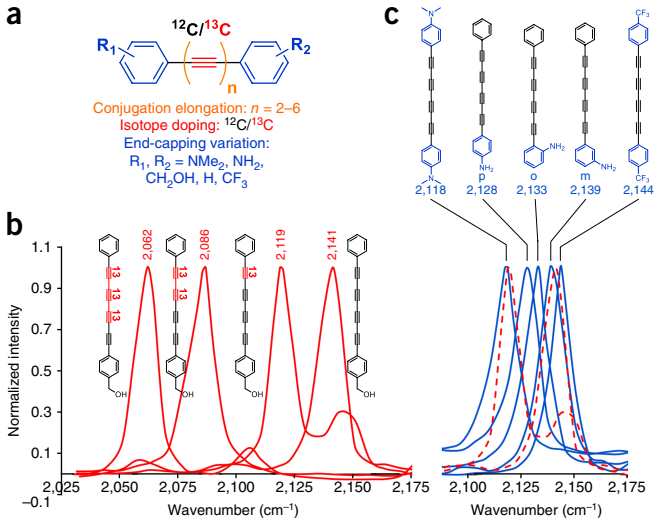

Figure 2 | Chemical strategies for Raman-frequency expansion of polyynes. (**a**) Frequency modulation on the unified polyyne scaffold by conjugation elongation, isotope doping and end-capping variations. (**b**) Frequency coarse-tuning with bond-selective ^{13}C isotope labeling (in red). (**c**) Frequency fine-tuning with electron-donating and electron-withdrawing groups (in blue). The dashed red spectra are the 2,119 cm^{-1} and 2,141 cm^{-1} peaks from **b**.

compounds in our study show good chemical stability under ambient conditions, as characterized by NMR and mass spectrometry.

These phenyl-capped polyynes exhibit unique vibrational spectroscopic properties. They all display an intense Raman peak with narrow linewidth (13 cm^{-1}) (**Fig. 1a**), originated from a collective out-of-phase bond-length alternation oscillation of both single and triple bonds[20]. Such a single sharp peak in the Raman-silent spectral region promises sensitive and specific detection. In addition, as the number of triple bonds increases from two to six, the Raman intensity grows superlinearly with a power-law exponent of 2.77 ± 0.06 (**Fig. 1b**). This trend is similar to the dependence observed in the second hyperpolarizability of other conjugated oligomers[21], which suggests much higher detection sensitivity than a single alkyne[22]. More importantly, going from 2-yne to 6-yne, the peak frequencies of polyynes shift almost linearly from 2,226 cm^{-1} to 2,066 cm^{-1} (**Fig. 1c**), naturally separating these polyynes in the frequency domain. Therefore, the unique spectral features of a single intense peak, narrow linewidth and the natural frequency spacing of different lengths render these polyynes an ideal scaffold for optical multiplexing.

Engineering polyynes for frequency tuning and expansion

To achieve supermultiplexing, we sought to further engineer the polyynes to expand the number of vibrational frequencies (**Fig. 2a**). We first exploited isotope doping, which is an effective approach to modify the reduced mass of the vibrational mode[23,24]. With multiple triple bonds present in polyynes, we optimized the ^{13}C-labeling pattern and were capable of modularly doping one or more triple bonds synthetically. The frequency-shifting effect of doping multiple triple bonds appears to be additive, as illustrated by singly, doubly and triply ^{13}C-labeled 4-yne series (**Fig. 2b**). Thus, such bond-selective ^{13}C doping allows us to tune the frequency in a range of 20–80 cm^{-1} (**Fig. 2b**). We noted the appearance of minor peaks and attributed it to the breakdown of centrosymmetry with nonuniform ^{13}C labeling and the violation of mutual Raman-IR exclusion[25].

We pursued an additional frequency modulation strategy, as bond-selective ^{13}C doping only offers coarse tuning with relatively large increments. Theory suggests that enhanced π-electron delocalization can increase electron–phonon coupling, which will weaken the stretching force constant of the vibrational mode and red shift the peak position[20]. We hypothesize that substituting the end-capping phenyl ring with electron-donating or electron-withdrawing groups might tune the vibrational frequency by influencing π-electron delocalization on the polyyne chain (**Fig. 2c**). Indeed, with electron-donating dimethylamine $-N(CH_3)_2$, doubly substituted 4-yne shows a significant redshift of 23 cm^{-1}, whereas the electron-withdrawing trifluoromethyl $-CF_3$ blue shifts by 3 cm^{-1}, compared to 4-yne at 2,141 cm^{-1}. The exact substitution position also matters. With the same $-NH_2$, para-position shows the largest redshift (2,128 cm^{-1}) due to the strong mesomeric effect. Ortho-position (2,133 cm^{-1}) is next, and meta-position (2,139 cm^{-1}) is the weakest. Thus, end-capping substitution provides the frequency fine-tuning (2–20 cm^{-1}), which is complementary to the coarse-tuning (20–80 cm^{-1}) from ^{13}C doping.

Polyynes with 20 resolvable frequencies: Carbow

Guided by the above principles, we synthesized a library of polyynes for frequency supermultiplexing through rational combination

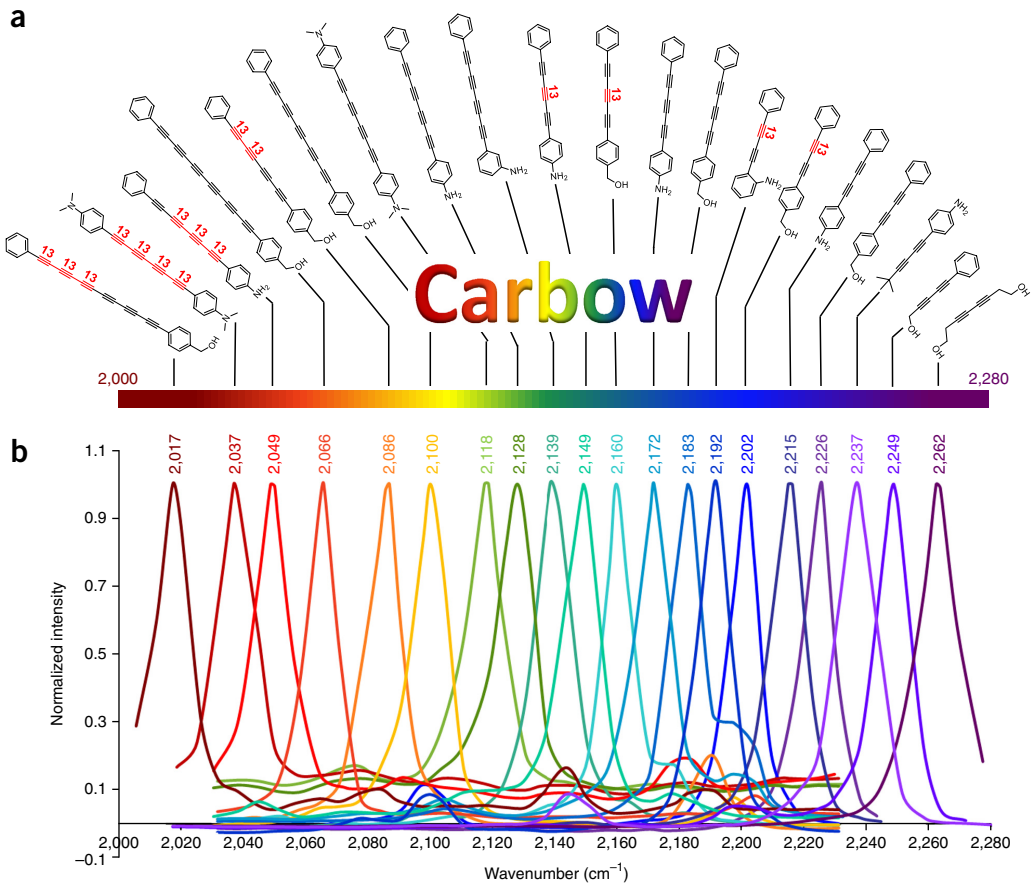

Figure 3 | Supermultiplexed polyynes. (**a**) Chemical structures of 20 polyynes with distinct Raman frequencies, which are termed Carbon rainbow (i.e., Carbow). (**b**) Raman peaks of Carbow in the silent spectral window.

of length modulation, bond-selective ^{13}C labeling and end-capping substitutions (**Supplementary Fig. 2**). We selected 20 structures with distinct Raman frequencies and termed them 'Carbon rainbow' (Carbow, **Fig. 3**), representing the largest number of resolvable frequency in the Raman-silent window. Note that using alkyl instead of phenyl as additional end-capping group can blue shift further to 2,262 cm^{-1}. Combined with six reported Raman frequencies in the fingerprint region from commercial dyes[26] and four commonly available fluorescent channels, 30 colors are resolvable, which, to our knowledge, is the highest reported for parallel optical detection. Compared to 14 MARS dyes recently reported in this range[26], Carbow peaks are more evenly spaced and well resolved with substantially less cross-talk. For instance, the spectral separation of the closest Carbow peaks nearly doubles that in the MARS dyes.

Optical imaging in cells with Carbow

The multiplexing capability of Carbow is useful in biological imaging for the simultaneous visualization of multiple species. We first characterized the detection sensitivity of Carbow using stimulated Raman scattering (SRS) microscopy with ultrahigh sensitivity and specificity[27]. We can detect as low as 630 nM of a 4-yne at a signal-to-noise ratio of 1 with a 1-ms time constant (<5 μM for most polyynes) under our SRS microscope (**Fig. 4a**). This is nearly 500 times more sensitive than previous SRS detection of a single alkyne tag[28]. Given the sub-μM sensitivity, we demonstrated immunostaining of specific proteins by conjugating polyynes to secondary antibodies for SRS imaging (**Fig. 4b** and **Supplementary Fig. 3**). We visualized the pattern of α-tubulin filament structures with good contrast. Tuning the wavelength away by 3 nm shows negligible background signal in the off-resonance channel. Such a sharp spectral feature is difficult to achieve for fluorescence approaches. Thus, Carbow is fully compatible with standard immunostaining procedures for protein-specific imaging.

We next demonstrated 15-color imaging of living cells (**Fig. 4c**), each of which is singularly stained with 1 of 15 colors (five fluorescent and ten Carbow molecules). All cells can be identified individually and unequivocally from the mixture in one 15-channel image without the need of complicated unmixing (**Supplementary Fig. 4**). Such resolvability would be challenging for fluorescence imaging with broad and overlapping spectra and for MARS dyes, which require a predetermined matrix for spectral unmixing owing to substantial cross-talk between channels[26]. Therefore, Carbow molecules enable optical imaging at a degree of multiplexing that is rarely reported for live cells with straightforward detection and analysis.

Supermultiplexed imaging of organelles in living cells

Further, owing to their neutral scaffold and high membrane permeability, Carbow molecules can be functionalized into live-cell, organelle-specific imaging probes. Through a carbamate linker on the phenyl ring, we introduced different targeting groups (**Fig. 4d–h**).

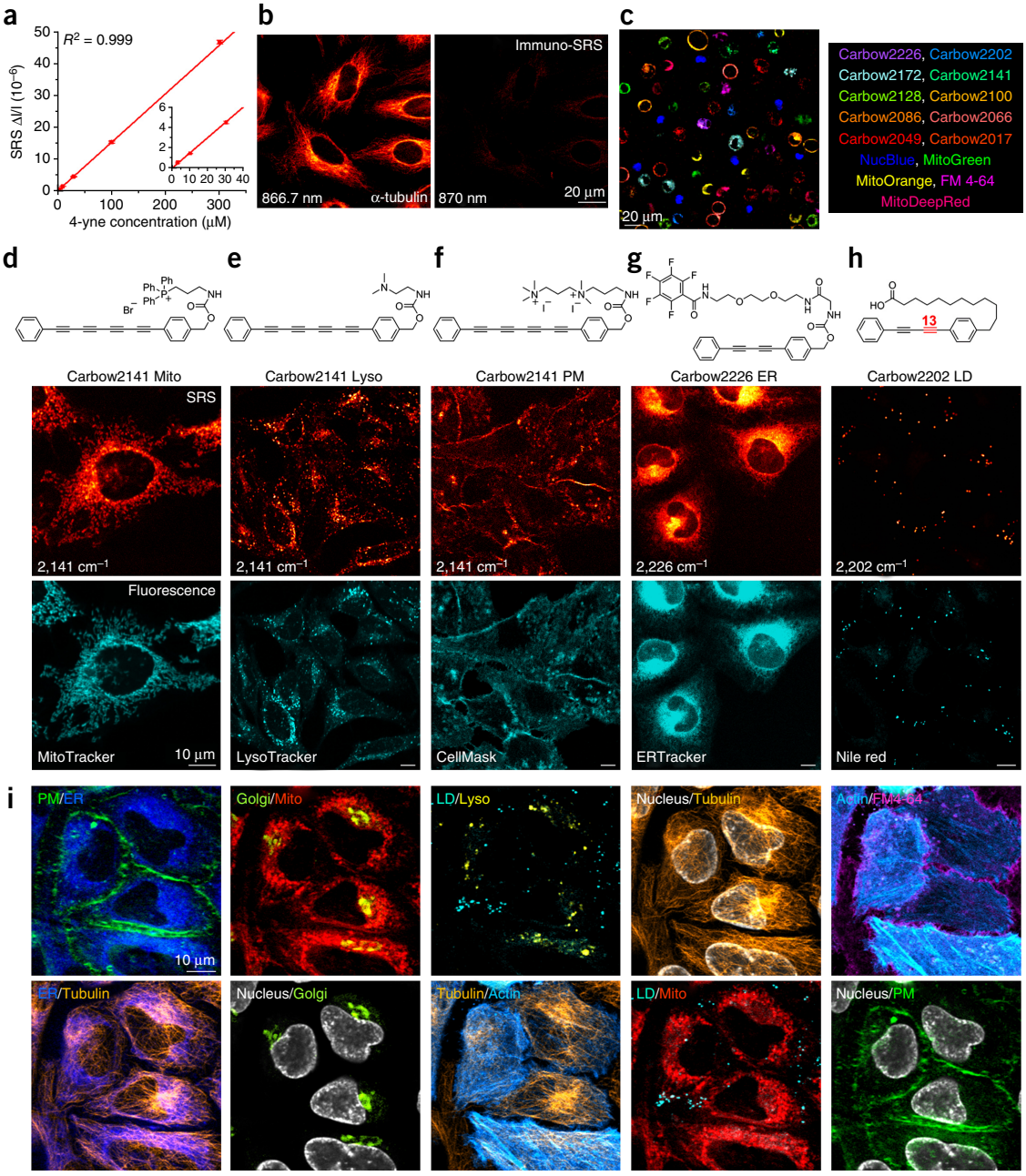

Figure 4 | Supermultiplexed optical imaging with polyynes. (**a**) Linear concentration dependence of 4-yne with sub-μM SRS detection sensitivity. Error bars, mean ± s.d.; $n = 3$ measurements. Solid line shows a linear fitting ($R^2 = 0.999$, $n = 5$ concentrations). Inset shows the same linear fitting at low concentrations. (**b**) Immunostaining and imaging of α-tubulin in fixed HeLa cells with 4-yne-conjugated antibody. The right panel shows the off-resonance image at 3 nm away. (**c**) 15-color tandem-fluorescence-SRS imaging of live HeLa cells with corresponding Carbow and fluorescent molecules. (**d**–**h**) Chemical structures of five organelle-targeted probes based on polyynes for live-cell imaging, including mitochondria (Mito, **d**), lysosome (Lyso, **e**), plasma membrane (PM, **f**), endoplasmic reticulum (ER, **g**) and lipid droplet (LD, **h**). (**i**) Ten-color optical imaging of PM (Carbow2141), ER (Carbow2226), Golgi (BODIPY TR), Mito (Carbow2062), LD (Carbow2202), Lyso (Carbow2086), nucleus (NucBlue), tubulin (SiR650), actin (GFP) and FM 4-64 in living HeLa cells. Overlay of two species are shown in each image.

Triphenylphosphonium (TPP^+) is a motif with high affinity to mitochondrial matrix due to the positive charge[29]. TPP^+ attached 4-yne (Carbow2141 Mito) shows specific localization to mitochondria (**Fig. 4d**). Lysosome lumen is acidic, where basic units are protonated and trapped inside, and thus we used a dimethylamine group to target Carbow2141 into lysosomes (Carbow2141 Lyso, **Fig. 4e**). Similarly, we chose a cationic diammonium group in Carbow2141 PM to stain the plasma membrane through interaction with anionic phosphate headgroups. Furthermore, we used a pentafluorobenzamide group with ethylene glycol chain in Carbow2226 ER to target the endoplasmic reticulum (**Fig. 4f**,**g**). Lastly, we attached a carboxylate-terminated C_{12} alkyl chain to Carbow2202 (Carbow2202 LD) to mimic fatty acids, and this probe is incorporated efficiently into lipid droplets (**Fig. 4h**). All five imaging probes show colocalized patterns with the corresponding fluorescent markers in live cells (**Supplementary Fig. 5** and **6**).

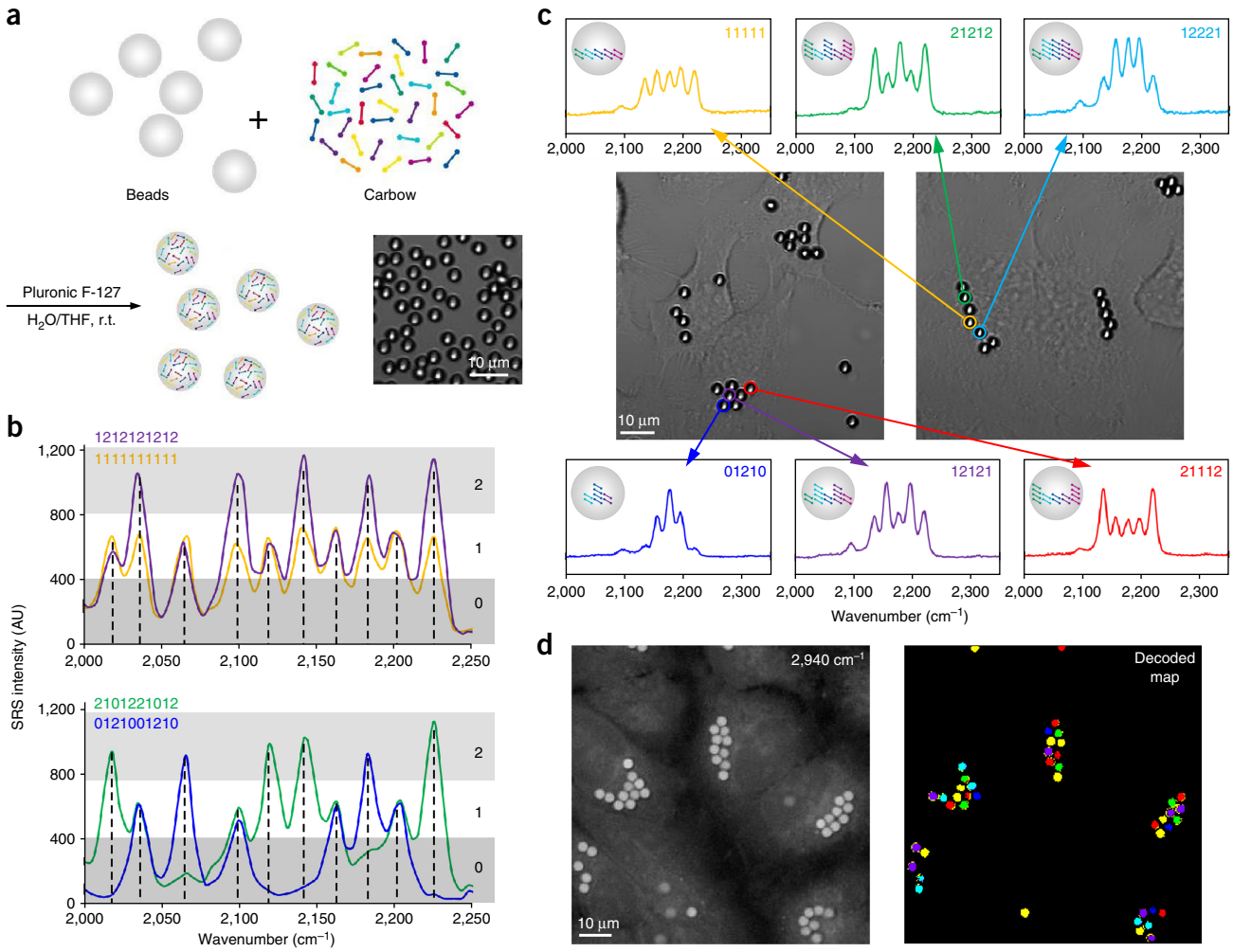

Figure 5 | Supermultiplexed optical barcoding with polyynes. (**a**) Polymer beads are encoded by combinatorial loading of polyynes. Inset shows the brightfield image of barcoded polystyrene beads. (**b**) Spectral barcoding of polyynes at ten frequencies and three intensities (0, or 1 or 2) with SRS readout. AU, arbitrary units. The italicized numbers 0, 1, and 2 indicate the three regions of digitized intensities. (**c**) Cells are labeled with multiple encoded beads as shown by the brightfield images. The barcode information is preserved in live HeLa cells with readout by spontaneous Raman measurement. The numbers at the top right indicate the digitized barcode information. (**d**) Decoding and spatial visualization of bead identities with SRS microscopy. Left, 2,940 cm^{-1} image of unidentified beads inside living HeLa cells; right, decoded beads in the field of view by hyperspectral SRS imaging at characteristic frequencies. The color of each bead (six different types) in the decoded map corresponds to the spectral barcode in **c**.

Carbow probes also exhibit high photostability (>98%) after 100 continuous frames (**Supplementary Fig. 7**) and little cytotoxicity (**Supplementary Fig. 8**).

We combined five organelle-targeted Carbow probes and five fluorescent reporters to achieve tandem ten-color optical imaging of subcellular structures in live cells (**Fig. 4i** and **Supplementary Table 1**; including plasma membrane, endoplasmic reticulum, Golgi, mitochondria, lysosome, lipid droplets, nucleus, tubulin and actin). Recognizing the essential roles of the organelle interactome in cellular activities, up to six-color organelle imaging has recently been achieved by fluorescence microscopy with spectral unmixing and color compensation[2]. We achieve ten-color organelle imaging in live cells without any unmixing or color compensation in image processing, which is difficult to achieve by other means. To our knowledge, this is the highest degree of multiplexing demonstrated for multitarget imaging inside living cells and relies critically on Carbow's well-resolved frequencies and live-cell compatibility.

Optical barcoding with combinatorial Carbow

Multiplexing can be useful in applications beyond imaging. Systems biology and personalized medicine benefit from high-throughput analysis of cells and biomolecules such as antigens and drugs, and the technology often requires distinguishable barcoding on micro-objects such as beads[7,30]. We hence applied Carbow to optical data storage (i.e., encoding) and identification (i.e., decoding). Harnessing polymer beads as the information carrier, we demonstrated that spectral barcoding with ten resolvable frequencies at three distinct intensity levels (i.e., ternary digit) is achievable using Carbow (**Fig. 5**). We loaded 3-μm-sized polystyrene beads with specified polyyne mixtures via a swelling–diffusion technique[31], and each bead was encoded with the desired spectral information in a single preparation step (**Fig. 5a**). As illustrated by four representative codes decoded by SRS readout, the intensity at each of the ten specified frequencies can be unambiguously digitalized as either 0, 1 or 2 (**Fig. 5b** and **Supplementary Table 2**). Spectral barcodes can also be read out by

conventional spontaneous Raman spectroscopy, and ten spectral patterns are decoded at the single-particle level (**Supplementary Fig. 9** and **Supplementary Table 3**). All nine combinations from two adjacent frequencies are well identified (**Supplementary Fig. 10**), demonstrating robustness against cross-talk. Thus, $3^{10} - 1 = 59{,}048$ distinct spectral barcodes can be generated, whereas the previous record[10] is around 1,000. Compared with previous optical barcoding materials, Carbow not only affords more resolvable frequencies, which benefit combinatorial coding exponentially, but is also free from photobleaching or complication of energy transfer as in fluorescence.

Besides *in vitro* detection, barcoded beads can potentially be used as a unique ID to tag individual cells. Owing to their small size, multiple beads can be combined in tagging a single cell. We show that HeLa cells can take up several beads containing different barcodes. The encoded information is retained inside live cells after 24 h and can be read out by spontaneous Raman spectroscopy (**Fig. 5c**). Furthermore, besides measuring the spectrum of one bead at a time, hyperspectral SRS imaging at discretized frequencies can decode all beads in the field of view (**Fig. 5d** and **Supplementary Fig. 11**), allowing rapid visualization of cellular identity. Hence, if using 3 encoded beads to tag each cell, we are able to generate ${}^{59,048}C_3 = 3 \times 10^{13}$ IDs, sufficient to barcode all cells in the human body (~10^{13} cells). This is orders of magnitudes greater than the limit of current state-of-the-art techniques based on organic dyes, quantum dots and upconversion nanocrystals or whispering-gallery mode detection of bead diameters[32].

DISCUSSION

We have engineered polyynes into imaging and barcoding probes for optical supermultiplexing, surpassing the existing 'multiplexing ceiling'. Compared to a recent report[26], the strong signals of polyynes arise from superlinear second hyperpolarizability enhancement of the linearly conjugated triple bonds under electronic nonresonant conditions, whereas MARS dyes derive their signals from electronic preresonant enhancement of planarly conjugated chromophores. In the applications demonstrated, we do not require stringent laser preresonance conditions, and we further expand and better separate frequencies with less cross-talk and no need of unmixing. Carbow probes are also more suitable for live-cell application and spectral barcoding because of their neutral scaffolds of polyynes. The current technology can be further improved. From a material perspective, more colors can be accessible with longer polyynes. The frequencies of polyynes can red shift toward 1,850 cm^{-1} with increasing length[33], providing an expanded window of 150 cm^{-1}. From a microscopy perspective, SRS imaging of single organelles in live cells can be achieved in as short as 2 s per frame (**Supplementary Fig. 12**), and high-speed hyperspectral SRS imaging[34,35] can be applied to capture fast dynamics of live cells. From a barcoding perspective, beads functionalized with antibodies or enzymes can be applied for medical diagnostics and drug discovery. SRS flow cytometry[36] can also be employed to detect tens of thousands of beads per second. In addition, using barcoded beads, the interactions of cells can potentially be mapped, for example, for the human cell atlas project. Lastly, as a proof of principle for identity security and anticounterfeiting applications, we demonstrate frequency encryption in a microscopic pattern (**Supplementary Fig. 13**). In summary, polyynes represent a class of optical material that could have wide applications in supermultiplexed cell imaging and sorting, barcoding, high-throughput screening and diagnosis, and identity security.

METHODS

Methods, including statements of data availability and any associated accession codes and references, are available in the online version of the paper.

Note: Any Supplementary Information and Source Data files are available in the online version of the paper.

ACKNOWLEDGMENTS

We are grateful for the discussion with L. Brus, Y. Shen and Z. Chen. W.M. acknowledges support from NIH Director's New Innovator Award (1DP2EB016573), R01 (EB020892), the US Army Research Office (W911NF-12-1-0594), and the Camille and Henry Dreyfus Foundation.

AUTHOR CONTRIBUTIONS

F.H. performed the spectroscopy, microscopy and biological studies and analyzed the data with the help of Y.M., L.W. and Q.X.; C.Z. performed the chemical synthesis together with R.L.; F.H. and W.M. conceived the concept; F.H., C.Z. and W.M. designed the experiments and wrote the manuscript with input from all authors.

COMPETING FINANCIAL INTERESTS

The authors declare competing financial interests: details are available in the online version of the paper.

1. Dean, K.M. & Palmer, A.E. Advances in fluorescence labeling strategies for dynamic cellular imaging. *Nat. Chem. Biol.* **10**, 512–523 (2014).
2. Valm, A.M. *et al.* Applying systems-level spectral imaging and analysis to reveal the organelle interactome. *Nature* **546**, 162–167 (2017).
3. Niehörster, T. *et al.* Multi-target spectrally resolved fluorescence lifetime imaging microscopy. *Nat. Methods* **13**, 257–262 (2016).
4. Krutzik, P.O. & Nolan, G.P. Fluorescent cell barcoding in flow cytometry allows high-throughput drug screening and signaling profiling. *Nat. Methods* **3**, 361–368 (2006).
5. Lu, J. *et al.* MicroRNA expression profiles classify human cancers. *Nature* **435**, 834–838 (2005).
6. Li, Y., Cu, Y.T.H. & Luo, D. Multiplexed detection of pathogen DNA with DNA-based fluorescence nanobarcodes. *Nat. Biotechnol.* **23**, 885–889 (2005).
7. Leng, Y., Sun, K., Chen, X. & Li, W. Suspension arrays based on nanoparticle-encoded microspheres for high-throughput multiplexed detection. *Chem. Soc. Rev.* **44**, 5552–5595 (2015).
8. Zijlstra, P., Chon, J.W. & Gu, M. Five-dimensional optical recording mediated by surface plasmons in gold nanorods. *Nature* **459**, 410–413 (2009).
9. Lu, Y. *et al.* Tunable lifetime multiplexing using luminescent nanocrystals. *Nat. Photonics* **8**, 32–36 (2014).
10. Nguyen, H.Q. *et al.* Programmable microfluidic synthesis of over one thousand uniquely identifiable spectral codes. *Adv. Opt. Mater.* **5**, 1600548 (2017).
11. Fournier-Bidoz, S. *et al.* Facile and rapid one-step mass preparation of quantum-dot barcodes. *Angew. Chem. Int. Ed. Engl.* **47**, 5577–5581 (2008).
12. Han, M., Gao, X., Su, J.Z. & Nie, S. Quantum-dot-tagged microbeads for multiplexed optical coding of biomolecules. *Nat. Biotechnol.* **19**, 631–635 (2001).
13. Cao, Y.C., Jin, R. & Mirkin, C.A. Nanoparticles with Raman spectroscopic fingerprints for DNA and RNA detection. *Science* **297**, 1536–1540 (2002).
14. Jin, R., Cao, Y.C., Thaxton, C.S. & Mirkin, C.A. Glass-bead-based parallel detection of DNA using composite Raman labels. *Small* **2**, 375–380 (2006).
15. Casari, C.S., Tommasini, M., Tykwinski, R.R. & Milani, A. Carbon-atom wires: 1-D systems with tunable properties. *Nanoscale* **8**, 4414–4435 (2016).
16. Hirsch, A. The era of carbon allotropes. *Nat. Mater.* **9**, 868–871 (2010).

17. Liu, M., Artyukhov, V.I., Lee, H., Xu, F. & Yakobson, B.I. Carbyne from first principles: chain of C atoms, a nanorod or a nanorope. *ACS Nano* **7**, 10075–10082 (2013).
18. Chalifoux, W.A. & Tykwinski, R.R. Synthesis of polyynes to model the sp-carbon allotrope carbyne. *Nat. Chem.* **2**, 967–971 (2010).
19. Luu, T. *et al.* Synthesis, structure, and nonlinear optical properties of diarylpolyynes. *Org. Lett.* **7**, 51–54 (2005).
20. Milani, A., Tommasini, M., Del Zoppo, M., Castiglioni, C. & Zerbi, G. Carbon nanowires: phonon and pi-electron confinement. *Phys. Rev. B* **74**, 153418 (2006).
21. Lucotti, A. *et al.* Absolute Raman intensity measurements and determination of the vibrational second hyperpolarizability of adamantyl endcapped polyynes. *J. Raman Spectrosc.* **43**, 1293–1298 (2012).
22. Yamakoshi, H. *et al.* Alkyne-tag Raman imaging for visualization of mobile small molecules in live cells. *J. Am. Chem. Soc.* **134**, 20681–20689 (2012).
23. Chen, Z. *et al.* Multicolor live-cell chemical imaging by isotopically edited alkyne vibrational palette. *J. Am. Chem. Soc.* **136**, 8027–8033 (2014).
24. Liu, Z. *et al.* Multiplexed multicolor Raman imaging of live cells with isotopically modified single walled carbon nanotubes. *J. Am. Chem. Soc.* **130**, 13540–13541 (2008).
25. Lucotti, A. *et al.* Evidence for solution-state nonlinearity of sp-carbon chains based on IR and Raman spectroscopy: violation of mutual exclusion. *J. Am. Chem. Soc.* **131**, 4239–4244 (2009).
26. Wei, L. *et al.* Super-multiplex vibrational imaging. *Nature* **544**, 465–470 (2017).
27. Freudiger, C.W. *et al.* Label-free biomedical imaging with high sensitivity by stimulated Raman scattering microscopy. *Science* **322**, 1857–1861 (2008).
28. Wei, L. *et al.* Live-cell imaging of alkyne-tagged small biomolecules by stimulated Raman scattering. *Nat. Methods* **11**, 410–412 (2014).
29. Yamakoshi, H. *et al.* A sensitive and specific Raman probe based on bisarylbutadiyne for live cell imaging of mitochondria. *Bioorg. Med. Chem. Lett.* **25**, 664–667 (2015).
30. Wilson, R., Cossins, A.R. & Spiller, D.G. Encoded microcarriers for high-throughput multiplexed detection. *Angew. Chem. Int. Ed. Engl.* **45**, 6104–6117 (2006).
31. Lee, J.H., Gomez, I.J., Sitterle, V.B. & Meredith, J.C. Dye-labeled polystyrene latex microspheres prepared via a combined swelling-diffusion technique. *J. Colloid Interface Sci.* **363**, 137–144 (2011).
32. Humar, M. & Yun, S.H. Intracellular microlasers. *Nat. Photonics* **9**, 572–576 (2015).
33. Agarwal, N.R. *et al.* Structure and chain polarization of long polyynes investigated with infrared and Raman spectroscopy. *J. Raman Spectrosc.* **44**, 1398–1410 (2013).
34. Ozeki, Y. *et al.* High-speed molecular spectral imaging of tissue with stimulated Raman scattering. *Nat. Photonics* **6**, 845–851 (2012).
35. Liao, C.S. *et al.* Microsecond scale vibrational spectroscopic imaging by multiplex stimulated Raman scattering microscopy. *Light Sci. Appl.* **4**, e265 (2015).
36. Zhang, C. *et al.* Stimulated Raman scattering flow cytometry for label-free single-particle analysis. *Optica* **4**, 103–109 (2017).

ONLINE METHODS

Chemical synthesis. Methods for chemical synthesis and characterization of all new compounds can be found in the **Supplementary Note**.

Stimulated Raman scattering microscopy. An integrated laser system (picoEMERALD, Applied Physics & Electronics, Inc.) was used to produce two synchronized laser beams at 80 MHz repetition rate. A fundamental Stokes beam (1,064 nm, 6 ps pulse width) was intensity modulated at 8 MHz by an electro-optic-modulator with >90% modulation depth, and a tunable pump beam (720–990 nm, 5–6 ps pulse width) was produced by a built-in optical parametric oscillator. The pump and Stokes beams were spatially and temporally overlapped using two dichroic mirrors and a delay stage inside the laser system and coupled into an inverted laser-scanning microscope (FV1200, Olympus) with optimized near-IR throughput.

The lasers were focused on the sample through a 25× water objective (XLPlan N, 1.05 NA MP, Olympus) or a 60× water objective (UPlanAPO/IR, 1.2 NA, Olympus) with high near-IR transmission. The beam sizes of pump and Stokes laser were adjusted to match the back aperture of the objective. After the sample, both beams were effectively collected by a high-NA oil condenser lens (1.4 NA, Olympus) in Kohler illumination, and the laser-scanning motion was descanned with a telescope. By blocking the Stokes beam with a high OD bandpass filter (890/220 CARS, Chroma Technology), only the pump beam was detected by a large-area (10 mm × 10 mm) silicon photodiode (FDS1010, Thorlabs) reverse biased at 64 DC voltage to maximize saturation threshold and response bandwidth. The output current of photodiode was filtered with an 8 MHz electronic bandpass filter (KR 2724, KR electronics) and terminated with 50 Ω before entering a RF lock-in amplifier (SR844, Stanford Research Systems or HF2LI, Zurich instrument).

The stimulated Raman loss signal was extracted from the pump beam by demodulation at the 8 MHz frequency with near-short-noise-limited sensitivity. The in-phase signal from the lock-in amplifier at each pixel was sent to the analog interface box (FV10-ANALOG, Olympus) of the microscope to generate the SRS image by scanning across the whole field of view. SRS images were acquired using 25× objective with 30 μs time constant from the lock-in amplifier and 100 μs pixel dwell time (10.2 s per 320 × 320 frame) unless otherwise specified. Measured after the objective, the pump power was from 12–48 mW, and the Stokes power was from 40–120 mW for all cell images (**Fig. 4**). For bead (**Fig. 5d** and **Supplementary Fig. 11**) and pattern (**Supplementary Fig. 13**) imaging, the pump power was from 12–24 mW, and the Stokes power was 20 mW. For immunoimaging (**Fig. 4b** and **Supplementary Fig. 3**), 100 μs time constant and 200 μs pixel dwell time were used. Ten-color live-cell organelle imaging (**Fig. 4i**) was performed using 60× objective and 80 μs time constant. Photostability experiments (**Supplementary Fig. 7**) were performed with 3 μs time constant and 4 μs pixel dwell time (0.4 s per 320 × 320 frame). Stimulated Raman scattering spectra were acquired by scanning the pump beam across the selected wavelength range point by point.

All brightfield and fluorescence images were collected using the Olympus FV1200 confocal microscope with CW laser excitation (488, 543 and 635 nm) and standard bandpass filter sets. Two-photon fluorescence images of NucBlue were collected with 780 nm pump laser excitation and detected by nondescanned photomultiplier tubes. All images were analyzed and assigned color by ImageJ.

Spontaneous Raman spectroscopy. Raman spectra were collected with the LabSpec 6 software on a confocal Raman microscope (Xplora, Horiba Jobin Yvon) at room temperature. The samples were excited through a 50× air objective (MPlan N, 0.75 NA, Olympus) by a 532-nm diode laser (27 mW after the objective). The acquisition time for bead solution samples (**Supplementary Figs. 9** and **10**) was 5 s and for beads in live cells (**Fig. 5c**) was 10 s.

Secondary-antibody conjugation with 4-yne Sulfo-NHS ester. Goat-anti-Rabbit secondary antibody solution (2 mg/mL, Millipore, AP132) was adjusted to pH ~8.3 with sodium bicarbonate solution. 50 μL 4 mg/mL 4-yne Sulfo-NHS ester in DMSO solution was added dropwise to 250 μL protein solution while stirring. Reaction was kept under gentle stirring at room temperature for 1 h. The labeled antibodies were purified using gel permeation chromatography with Sephadex G-25 (Sigma, G25150). Sephadex G-25 gel was first swelled in PBS buffer at 90 °C for 1 h and settled down at room temperature. The gel was then exchanged with fresh PBS buffer and stored at 4 °C. For gel chromatography, the column (diameter ≈ 1 cm and length > 12 cm) was loaded with swelled gels and equilibrated with PBS buffer. The antibody solution was applied and eluted with PBS. The first band with light color for 4-yne-conjugated antibodies was collected. The solution was then centrifuged briefly, and the supernatant was concentrated using Amicon Ultra Centrifugal Filters (Millipore, UFC501096) to a final concentration of ~2 mg/mL in PBS with 5 mM sodium azide and stored at −20 °C.

Sample preparations for stimulated Raman scattering and fluorescence imaging. HeLa and COS-7 cells were cultured with DMEM medium (Invitrogen, 11965) supplemented with 10% FBS (Invitrogen, 16000) and 1% penicillin–streptomycin (Invitrogen, 15140). All cell cultures were maintained in a humidified environment at 37 °C and 5% CO_2.

All samples were assembled into a chamber using an imaging spacer (Sigma, GBL654008) filled with PBS solution for imaging.

Immunostaining for stimulated Raman scattering imaging in fixed HeLa cells. HeLa cells were seeded on a glass coverslip in a 4-well plate with ~1 mL of culture media for 24 h. Cells were fixed with 4% PFA for 20 min or methanol for 25 min, washed with 10% goat serum supplemented with 1% bovine serum albumin (BSA) and 0.3 M glycine twice, and permeabilized with 0.1% Tween PBS solution for 40 min. Primary antibody in rabbit (Anti-α-tubulin, Abcam ab18251; Anti-Histone H2B, Abcam ab1790; Anti-Tom20, Santa Cruz Biotechnology sc-11415) was added to the cells at 1:50 dilution in 3% BSA solution and incubated overnight at 4 °C. The cells were then blocked with 10% goat serum for 30 min and incubated with 4-yne conjugated goat-anti-rabbit secondary antibody by 1:25 dilution in 10% goat serum at 4 °C overnight. The cells were washed with PBS twice before imaging (**Fig. 4b** and **Supplementary Fig. 3**).

15-color imaging of live Hela cells with supermultiplexed polyynes. HeLa cells were separately seeded in 15 wells of a

24-well plate for 24 h. Each well was labeled with a single color of fluorescent dyes or polyynes in culture media at 37 °C, including Carbow2226 Mito (5 μM), Carbow2172 (3 μM), Carbow2141 (10 μM), Carbow2128 (2 μM), Carbow2100 (4 μM), Carbow2086 (10 μM), Carbow2066 (10 μM), Carbow2049 (5 μM), and Carbow2017 (10 μM) for 4 h; Carbow2202 LD (4 μM) for 24 h;MitoTracker Green (100 nM, Invitrogen, M7514), MitoTracker Orange CMTMRos (50 nM, Invitrogen, M7510), and MitoTracker Deep Red (50 nM, Invitrogen, M22426) for 1 h; NucBlue Live ReadyProbes Reagent (1 drop, Invitrogen, R37605) and FM 4-64 (5 μg/mL, Invitrogen, T3166) for 30 min. All cells were then washed with PBS once, detached from each well with trypsin for 2 min, and mixed together in fresh culture media. The cell mixture was centrifuged at 1,000 r.p.m. for 1.5 min, and the cell pellet was mixed with PBS. Cells were added to the imaging chamber and settled for 1 h to reduce the movement before imaging, and each cell was maintained with a single color during the imaging period (**Fig. 4c** and **Supplementary Fig. 4**).

Mitochondria imaging in live HeLa or COS-7 cells with Carbow2141 Mito. Cells were cultured on a glass coverslip in a 4-well plate for 24 h, and 2 μM Carbow2141 Mito was added in the media for 1 h at 37 °C. Cells were washed with PBS for three times before imaging. For colocalization, 100 nM MitoTracker Deep Red was used to stain mitochondria for 1 h (**Fig. 4d**; **Supplementary Figs. 5** and **6**).

Lysosome imaging in live HeLa or COS-7 cells with Carbow2141 Lyso. Cells were cultured on a glass coverslip in a 4-well plate for 24 h, and 4 μM Carbow2141 Lyso was added to cells for 30 min at 37 °C. Cells were washed with PBS for three times before imaging. For colocalization, 100 nM LysoTracker Red (Invitrogen, L7528) was used to stain lysosome for 30 min (**Fig. 4e**; **Supplementary Figs. 5** and **6**).

Plasma-membrane imaging in live HeLa or COS-7 cells with Carbow2141 PM. Cells were cultured on a glass coverslip in a 4-well plate for 24 h, incubated with 3–5 μM Carbow2141 PM in the culture media for 20–30 min at 37 °C and washed with PBS for three times before imaging. For colocalization, 0.5 μg/mL CellMask Deep Red (Invitrogen, C10046) was used to stain cell membrane for 5 min (**Fig. 4f**; **Supplementary Figs. 5** and **6**).

Endoplasmic-reticulum imaging in live HeLa or COS-7 cells with Carbow2226 ER. Cells were cultured on a glass coverslip in a 4-well plate for 24 h and incubated with 10 μM Carbow2226 ER for 2 h at 37 °C. Cells were washed with PBS for three times before imaging. For colocalization, 1 μM ERTracker Green (Invitrogen, E34251) was used to stain endoplasmic reticulum for 2 h (**Fig. 4g**; **Supplementary Figs. 5** and **6**).

Lipid-droplet imaging in live HeLa or COS-7 cells with Carbow2202 LD. Cells were cultured on a glass coverslip in a 4-well plate for 24 h, and 10 μM Carbow2202 LD was added to cell media for overnight at 37 °C. Cells were washed with PBS for three times before imaging. For colocalization, 1 μM Nile red (Invitrogen, N1142) was used to stain lipid droplets for 10 min. (**Fig. 4h**; **Supplementary Figs. 5** and **6**).

Ten-color organelle-specific imaging in live Hela cells with polyyne probes. HeLa cells were seeded on a glass coverslip in a 4-well plate with culture media for 24 h, and actin-GFP plasmids (Invitrogen, C10582) were transfected into cells for 48 h before imaging according to Invitrogen protocol. 10 μM Carbow2202 LD was added in the culture media overnight at 37 °C before imaging. On the day of imaging, cells were incubated with 10 μM Carbow2226 ER and 0.02% Pluronic F-127 (Invitrogen, P3000MP) for 2 h, 2 μM Carbow2086 Lyso, 4 μM Carbow2062 Mito and 1 μM SiR-tubulin (Cytoskeleton, CY-SC002) for 1 h, 3 μM Carbow2141 PM and one drop of NucBlue for 20 min at 37 °C. 1 h before imaging, cells were labeled with 5 μM BODIPY TR Ceramide (Invitrogen D7540) and 0.1% Pluronic F-127 in Hanks' buffered salt solution (HBSS, Invitrogen, 14025) for 10 min at 37 °C. After the incubation, cells were washed with PBS solution twice, quickly immersed in 5 μg/mL FM 4-64 HBSS solution (without magnesium or calcium) on ice for 1 min before imaging (**Fig. 4i** and **Supplementary Table 1**).

Cell viability assays. HeLa cells were incubated with organelle-targeted polyynes at specified conditions or illuminated by SRS lasers. Cell viability assays were then performed using Live/Dead viability/cytotoxicity kit for mammalian cells (Invitrogen, L3224) by incubating with 2 μM calcein AM and 4 μM EthD-1 working solution for 20 min at 37 °C (**Supplementary Fig. 8**).

Spectral barcoding in polystyrene beads with supermultiplexed polyynes. 10 μL 3.0 μm polystyrene beads (10% in aqueous solution, Sigma, LB30) were mixed with 5 μL Pluronic F-127 (20% in DMSO) and 85 μL deionized water. Selected polyynes (in DMSO) were diluted to designated concentrations (**Supplementary Tables 2** and **3**) in a solution of 100 μL deionized water and 100 μL THF (Sigma, 401757). The polyyne THF–water solution was then mixed with 100 μL of bead and F-127 solution. After vortexing for 10 min, the mixture was further agitated on a shaker for 2 h at room temperature and then washed with deionized water three times. For live-cell labeling, barcoded beads were incubated in 1 wt% poly-L-lysine aqueous solution (M_w = 30,000–70,000, Sigma, P2636) for 30 min at room temperature and washed with water for three times before use.

Live-cell tagging with spectral barcoded beads. HeLa cells were seeded on a glass coverslip in a 4-well plate with culture media for 24 h. Cells were incubated with barcoded beads for 24 h before spontaneous Raman measurement (**Fig. 5c**) or SRS imaging (**Fig. 5d** and **Supplementary Fig. 11**). A custom MATLAB program was used to decode the spectral barcodes of beads in the whole field of view based on the hyperspectral SRS images.

Fabrication of microscopic pattern and frequency encryption with supermultiplexed polyynes. Poly(methyl methacrylate) (PMMA, 495K A4 + 950K A9, MicroChem) was spin coated onto Si/SiO_2 substrate and baked at 170 °C for 10 min. The substrate was exposed to e-beam lithography and a solution of developer to generate the microscopic pattern of Columbia logo. The polydimethylsiloxane (PDMS) precursor was prepared using Sylgard 184 Silicone Elastomer Kit (Fisher, NC9644388). Elastomer and curing agent (10:1 ratio) were mixed and poured onto the

doi:10.1038/nmeth.4578

patterned Si/SiO_2 substrate. After heating at 80 °C for 1 h, the PDMS pattern was peeled off the substrate.

Frequency encryption was carried out by immersing the PDMS with Columbia logo in ethanol solution (Fisher, BP2818) with specified polyynes (0.2–1.2 mM) as security codes at room temperature overnight. After ethanol evaporation, the pattern was rinsed with deionized water before imaging (**Supplementary Fig. 13**).

Statistics. For correlation analysis in spectroscopy measurements (**Figs. 1b** and **4a**), least-squares regression is applied with Origin software. Reported *n* values represent the number of compounds (**Fig. 1b**) and concentrations (**Fig. 4a**) measured independently in the experiments. For the immunostaining and imaging experiments (**Fig. 4b**), experiments were repeated four times independently with similar results. For the 15-color imaging experiments (**Fig. 4c**), experiments were repeated three times independently with similar results. For the live-cell, organelle-targeted experiments (**Fig. 4d**–**h**), experiments were repeated five times independently with similar results. For the ten-color organelle-targeted imaging (**Fig. 4i**), experiments were repeated three times independently with similar results. For the bead labeling in live cells by spontaneous Raman readout (**Fig. 5c**) or SRS imaging (**Fig. 5d**), experiments were repeated three times independently with similar results.

Code availability. The MATLAB code is available from the corresponding author upon request.

Life Sciences Reporting Summary. Further information on experimental design is available in the **Life Sciences Reporting Summary**.

Data availability. The data that support the findings of this study are provided in **Supplementary Figures 1**–**13**, **Supplementary Tables 1**–**3** and **Supplementary Note 1** and are available from the corresponding author upon request.

nature research

Corresponding author(s): Wei Min

☐ Initial submission ☐ Revised version ☒ Final submission

Life Sciences Reporting Summary

Nature Research wishes to improve the reproducibility of the work that we publish. This form is intended for publication with all accepted life science papers and provides structure for consistency and transparency in reporting. Every life science submission will use this form; some list items might not apply to an individual manuscript, but all fields must be completed for clarity.

For further information on the points included in this form, see Reporting Life Sciences Research. For further information on Nature Research policies, including our data availability policy, see Authors & Referees and the Editorial Policy Checklist.

Experimental design

1. Sample size

Describe how sample size was determined.

The results of the study demonstrate the multiplexing capability of the method, and don't depend on the statistical variation of the sample properties. A sample size determination was not done.

2. Data exclusions

Describe any data exclusions.

No data were excluded from the analyses.

3. Replication

Describe whether the experimental findings were reliably reproduced.

The method was applied in various experiments. Multiple experiments were repeated with similar results as reported in the Methods and figure legends.

4. Randomization

Describe how samples/organisms/participants were allocated into experimental groups.

This is not relevant for the method, because it doesn't depend on the statistical variation of the sample properties.

5. Blinding

Describe whether the investigators were blinded to group allocation during data collection and/or analysis.

This is not relevant for the method, because it doesn't depend on the statistical variation of the sample properties.

Note: all studies involving animals and/or human research participants must disclose whether blinding and randomization were used.

6. Statistical parameters

For all figures and tables that use statistical methods, confirm that the following items are present in relevant figure legends (or in the Methods section if additional space is needed).

n/a	Confirmed	
☐	☒	The exact sample size (*n*) for each experimental group/condition, given as a discrete number and unit of measurement (animals, litters, cultures, etc.)
☐	☒	A description of how samples were collected, noting whether measurements were taken from distinct samples or whether the same sample was measured repeatedly
☐	☒	A statement indicating how many times each experiment was replicated
☐	☒	The statistical test(s) used and whether they are one- or two-sided (note: only common tests should be described solely by name; more complex techniques should be described in the Methods section)
☒	☐	A description of any assumptions or corrections, such as an adjustment for multiple comparisons
☐	☒	The test results (e.g. *P* values) given as exact values whenever possible and with confidence intervals noted
☐	☒	A clear description of statistics including central tendency (e.g. median, mean) and variation (e.g. standard deviation, interquartile range)
☐	☒	Clearly defined error bars

See the web collection on statistics for biologists for further resources and guidance.

Nature Methods: doi:10.1038/nmeth.4578

Software

Policy information about availability of computer code

7. Software

Describe the software used to analyze the data in this study.	Images were collected with Olympus FV1200. Raman spectra were collected with LabSpec 6 software. ImageJ 1.48b, OriginPro 8 and MATLAB R2012a were used to analyze the data.

For manuscripts utilizing custom algorithms or software that are central to the paper but not yet described in the published literature, software must be made available to editors and reviewers upon request. We strongly encourage code deposition in a community repository (e.g. GitHub). *Nature Methods* guidance for providing algorithms and software for publication provides further information on this topic.

Materials and reagents

Policy information about availability of materials

8. Materials availability

Indicate whether there are restrictions on availability of unique materials or if these materials are only available for distribution by a for-profit company.	All unique materials used are available to nonprofit researchers from the authors on request.

9. Antibodies

Describe the antibodies used and how they were validated for use in the system under study (i.e. assay and species).	Anti-alpha tubulin antibody in rabbit was purchased from Abcam, ab18251. Anti-Histone H2B antibody in rabbit was purchased from Abcam, ab1790. Anti-Tom20 antibody in rabbit was purchased from Santa Cruz Biotechnology, sc-11415. Goat-anti-Rabbit secondary antibody solution was purchased from Millipore, AP132. All antibodies are validated by vendors.

10. Eukaryotic cell lines

a. State the source of each eukaryotic cell line used.	All cell lines were obtained from ATCC.
b. Describe the method of cell line authentication used.	Cell lines were authenticated by ATCC.
c. Report whether the cell lines were tested for mycoplasma contamination.	Cell lines were tested negative for mycoplasma contamination.
d. If any of the cell lines used are listed in the database of commonly misidentified cell lines maintained by ICLAC, provide a scientific rationale for their use.	No commonly misidentified cell lines were used.

Animals and human research participants

Policy information about studies involving animals; when reporting animal research, follow the ARRIVE guidelines

11. Description of research animals

Provide details on animals and/or animal-derived materials used in the study.	No animals were used.

Policy information about studies involving human research participants

12. Description of human research participants

Describe the covariate-relevant population characteristics of the human research participants.	The study did not involve human research participants.

Nature Methods: doi:10.1038/nmeth.4578